

1 **Measurement report: Characteristics of**
2 **nitrogen-containing organics in PM_{2.5} in Urumqi,**
3 **northwest China: differential impacts of**
4 **combustion of fresh and old-age biomass**
5 **materials**

6

7 Yi-Jia Ma¹, Yu Xu^{2,*}, Ting Yang¹, Hong-Wei Xiao², Hua-Yun Xiao²

8

9 ¹School of Environmental Science and Engineering, Shanghai Jiao Tong University,
10 Shanghai 200240, China

11 ²School of Agriculture and Biology, Shanghai Jiao Tong University, Shanghai 200240,
12 China

13

14

15

16

17

18

*Corresponding authors

19

Yu Xu

20

E-mail: xuyu360@sjtu.edu.cn

21

22

23

24

25 **Abstract:** Nitrogen-containing organic compounds (NOCs) are abundant and
26 important aerosol components deeply involved in the global nitrogen cycle. However,
27 the sources and formation processes of NOCs remain largely unknown, particularly in
28 the city (Urumqi, China) farthest from the ocean worldwide. Here, NOCs in PM_{2.5}
29 collected in Urumqi over a one-year period were characterized by ultrahigh-resolution
30 mass spectrometry. The abundance of CHON compounds (mainly poor-O unsaturated
31 aliphatic-like species) in the positive ion mode was higher in the warm period than in
32 the cold period, which was largely attributed to the contribution of fresh biomass
33 material combustion (e.g., forest fires) associated with amidation of unsaturated fatty
34 acids in the warm period, rather than the oxidation processes. However, CHON
35 compounds (mainly nitro-aromatic species) in the negative ion mode increased
36 significantly in the cold period, which was tightly related to old-age biomass
37 combustion (e.g., dry straws) in wintertime Urumqi. For CHN compounds, alkyl nitriles
38 and aromatic species showed higher abundance in the warm and cold periods,
39 respectively. Alkyl nitriles can from fresh biomass material combustion associated with
40 the dehydration of amides (the main CHON compounds in the warm period). In contrast,
41 aromatic species were tightly related to old-age biomass burning. These findings further
42 suggested different impacts of the combustion of fresh- and old-age biomass materials
43 on NOC compositions in different seasons. The overall results shed light on the
44 mechanisms by which fresh and old-age biomass materials release different NOCs
45 during combustion.

46 **Keywords:** Aerosols, Organic nitrogen, Molecular composition, Fresh biomass, Old-

47 age biomass

48 **1. Introduction**

49 Fine particulate matter (PM_{2.5}) is a typical atmospheric pollutant that can affect the
50 global climate system, as well as urban air quality and human health (Seinfeld et al.,
51 2016; Wang et al., 2021a). Organic aerosol (OA) contributes significantly (20–90%) to
52 PM_{2.5} mass concentration in most polluted areas worldwide (Zhang et al., 2007; Han et
53 al., 2023). However, up to 77% of molecules in OA include nitrogen-containing
54 functional groups (Ditto et al., 2020; Kenagy et al., 2021), which have been suggested
55 to play important roles in the formation, transformation, acidity, and hygroscopicity of
56 OA (Xu et al., 2020; Wang et al., 2017b; Laskin et al., 2009). Moreover, the further
57 oxidation or nitrification of some nitrogen-containing organic compounds (NOCs) and
58 volatile organic compounds (VOCs) by ozone (O₃), hydroxyl radical (•OH), and
59 nitrogen oxide (NO_x) can lead to an increase in the health hazards of OA (Franze et al.,
60 2005; Bandowe and Meusel, 2017). Nitrated amino acids and nitrated PAHs are two
61 representative hazard NOCs (Franze et al., 2005; Bandowe and Meusel, 2017). Thus,
62 the identification of aerosol NOCs at the molecular level is important for improving our
63 understanding of the precursors, sources, and formation processes of nitrogen-
64 containing OA.

65 Previous observations in urban, rural, marine, and forest areas have suggested that
66 the molecular composition and relative abundance of aerosol NOCs were spatially
67 different (Samy and Hays, 2013; Jiang et al., 2022; Lin et al., 2012; Xu et al., 2023;
68 Luo et al., 2023; Zeng et al., 2021; Zhang et al., 2022; Zeng et al., 2020). These

69 differences can be mainly attributed to the diverse sources and formation mechanisms
70 of aerosol NOCs. Commonly reported primary sources include combustion process
71 releases and natural emissions (e.g., soils, plant debris, pollen, and ocean) (Song et al.,
72 2022; Wang et al., 2017b; Cape et al., 2011; Lin et al., 2023). In addition, aerosol NOCs
73 can also be tightly associated with secondary formation processes involving the
74 reactions of reactive nitrogen with VOCs or particle-phase CHO compounds (Bandowe
75 and Meusel, 2017; Zarzana et al., 2012; Laskin et al., 2014). For example, laboratory
76 experiments have suggested that the oxidation of isoprene and α -/ β -pinene in the
77 presence of NO_x can result in the formation of organic nitrates (e.g., methacryloyl
78 peroxyxynitrate, dihydroxynitrates, and monohydroxynitrates) (Surratt et al., 2010;
79 Rollins et al., 2012; Nguyen et al., 2015). The reduced nitrogen species (e.g., NH_3 , NH_4^+ ,
80 and organic amines) have been demonstrated to contribute to the formation of NOCs
81 through "carbonyl-to-imine" transformations in the laboratory experiments (Zarzana et
82 al., 2012; Laskin et al., 2014). In the field observation studies, NOCs in particulate
83 matter were analyzed at the molecular level to indicate their sources and formation
84 mechanisms (Jiang et al., 2022; Lin et al., 2012; Zhong et al., 2023). Xu et al. (2023)
85 characterized the variations of molecular compositions in urban road $\text{PM}_{2.5}$, suggesting
86 that organic nitrates increased largely through the interactions of atmospheric oxidants,
87 reactive gas-phase organics, and aerosol liquid water. Several field studies conducted
88 in Beijing (China) and Guangzhou (China) also suggested that the molecular
89 compositions and formation of NOCs were tightly associated with environmental
90 conditions (Jiang et al., 2022; Lin et al., 2012; Xie et al., 2020). Generally, most studies

91 on aerosol NOCs were performed in economically developed regions, as well as in
92 forest and marine areas (Jiang et al., 2022; Wang et al., 2017a; Ditto et al., 2022b; Altieri
93 et al., 2016; Xu et al., 2020; Liu et al., 2023; Zhang et al., 2022; Zeng et al., 2020). In
94 contrast, few studies have investigated the sources and atmospheric transformation of
95 NOCs in the northwest border urban of China (e.g., Urumqi) with fragile ecology and
96 harsh environmental conditions (e.g., cold winter and dry summer), which may hinder
97 our comprehensive and in-depth understanding of the formation process of NOCs in
98 ambient aerosols.

99 Biomass burning emissions were widely reported in the source identification of
100 aerosol NOCs in northern and southwestern China because of heating and cooking
101 needs (Zhong et al., 2023; Wang et al., 2021c; Chen et al., 2017). A recent observation
102 study in urban Tianjin suggested that most CHON compounds in wintertime PM_{2.5}
103 originated from biomass burning (Zhong et al., 2023). The CHN₂ compounds have been
104 identified in biomass burning OA (BBOA) (Laskin et al., 2009; Wang et al., 2017b).
105 Moreover, the high temperature generated by biomass burning can facilitate the release
106 of ammonia, a process that caused the reaction of carboxylic acids (e.g., oleic acid) with
107 ammonia to form amides and alkyl nitriles (Radzi Bin Abas et al., 2004; Simoneit et al.,
108 2003). Interestingly, we found that biomass burning in rural China typically includes
109 fresh biomass materials (e.g., forest fires) and old-age biomass materials (e.g., straw
110 after autumn harvest, fallen leaf, and deadwood). Fresh biomass is rich in oils and
111 proteins, whereas old-age biomass materials are usually oligotrophic due to the transfer
112 of nutrients to tender tissues or fruits (Jian et al., 2016; Xu and Xiao, 2017). Thus, NOCs

113 released from different types of biomass combustion may vary in molecular
114 compositions. However, there are large gaps in our current knowledge about the
115 impacts of fresh and old-age biomass burning on NOCs in ambient aerosols.

116 Urumqi (northwest China) is the largest inland city farthest from the ocean in the
117 world, which is becoming increasingly prominent due to the national strategy of the
118 "One Belt, One Road." The city and neighboring countries have a dry summer that can
119 easily trigger forest fires (Bátori et al., 2018; Xu et al., 2021), while the winter is
120 freezing with intensive old-age biomass and fuel combustion for heating (Ren et al.,
121 2017). In this study, we presented one-year ambient measurements of the chemical
122 compositions in PM_{2.5} collected from Urumqi. The specific aims of this study are (1) to
123 investigate the molecular-level speciation of functionalized organic nitrogen
124 compounds via high-resolution mass spectrometry with positive (ESI+) and negative
125 (ESI-) ionizations and (2) to investigate the potential sources and formation processes
126 for NOCs with a special focus on the relative influences of fresh and old-age biomass
127 burning in different seasons.

128

129 **2. Materials and methods**

130 **2.1. Study site description and sample collection**

131 The study was conducted in Urumqi city, which has an average altitude of 800 m.
132 The region has an arid temperate continental climate with an annual mean temperature
133 of 7.4 ± 13.9 °C and an annual mean rainfall of 27.8 mm. The sampling site is located
134 in the suburban area (Boda campus of Xinjiang University) of the city (87.75°E,

135 43.86°N) (**Figure S1**), which is characterized by low population and traffic density.
136 This is because Urumqi is relatively vast and sparsely populated compared to developed
137 coastal cities in China (Qizhi et al., 2016). Additionally, the area is surrounded by
138 mountains on three sides, resulting in the difficulty in diffusing air pollutants. The
139 dominant forest trees in this area are *Picea schrenkiana*, *Betula tianschanica* Rupr.,
140 *Populus talassica* Kom., and *Ulmus pumila* L.. The dry climate and strong sunlight in
141 the warm period ($18.81 \pm 6.4^\circ\text{C}$, **Table S1**) would be the main culprits of forest fires in
142 the local and nearby areas. In the cold period ($-1.96 \pm 11.26^\circ\text{C}$) (**Table S1**), the
143 centralized heating and old-age biomass burning may be the main contributors to local
144 air pollution. Thus, it provides an unexpected opportunity to investigate the potentially
145 differential impacts of fresh and old-age biomass burning on aerosol NOCs.

146 A high-volume air sampler (Series 2031, Laoying, China) was set up on the
147 rooftop of a building (School of Geology and Mining Engineering, Xinjiang University).
148 PM_{2.5} samples ($n = 73$) were collected every five days with a duration of ~24 h onto
149 prebaked (450 °C for ~ 10 h) quartz fiber filters (Pallflex, Pall Corporation, USA) from
150 1 March 2018 to 26 February 2019. One blank filter was collected every month ($n =$
151 12). All filter samples were stored at -30°C until further analysis. During the sampling
152 campaigns, the meteorological data (e.g., temperature and relative humidity) and the
153 concentrations of O₃ and NO_x were recorded daily from the adjacent environmental
154 monitoring station. In addition, the trajectories (72 h) of air masses arriving at the
155 sampling site at each sampling event were calculated to investigate the potential
156 influence of pollutant transport on aerosol NOCs.

157

158 **2.2. Chemical analysis**

159 A portion of each filter sample was extracted twice using methanol (LC-MS grade,
160 CNW Technologies Ltd.) under sonication in a chilled ice slurry (~ 4 °C). The extracted
161 solutions were filtered through a polytetrafluoroethylene syringe filter ($0.22\ \mu\text{m}$, CNW
162 Technologies GmbH). Subsequently, the extracts were concentrated to $300\ \mu\text{L}$ with a
163 gentle stream of gaseous nitrogen (Shanghai Likang Gas Co., Ltd). The final extracts
164 were divided into two parts, which were analyzed separately as described in previous
165 study (Wang et al., 2021b) under ESI+ and ESI- modes using an UPLC-ESI-QToFMS
166 (Xevo G2-XS QToFMS, Waters) system. It should be pointed out that UPLC-ESI-MS
167 (i.e., TOF-only) was used to identify molecular formulas of organic matter, while the
168 functional groups of the target molecule formulas were deciphered by UPLC-ESI-
169 MS/MS (i.e., tandem mass spectrometry). Ions obtained from m/z 50–700 were
170 assigned molecule formulas by assuming hydrogen or sodium adducts in ESI+ mode
171 and deprotonation in ESI- mode. Detailed chromatographic conditions, parameter
172 selection, and quality control were displayed in the Supplement (**Sect. S1**). Notably,
173 there may be differences in ionization efficiencies between compound types. However,
174 the exact impacts of ionization efficiency on multifunctional compounds in a complex
175 mixture are uncertain and difficult to evaluate (Ditto et al., 2022b; Yang et al., 2023).
176 Thus, the intercomparison across compound relative abundance without considering
177 potentially differentiated ionization efficiency was conducted in this study, which was
178 similar to many previous studies (Xu et al., 2023; Jiang et al., 2022).

179 For the measurement of inorganic ions, a portion of each filter sample was
180 ultrasonically extracted with Milli-Q water (18 MΩ cm) in an ice-water bath (~4 °C).
181 The extract solutions were then filtered via a polytetrafluoroethylene syringe filter (0.22
182 μm, Millipore, Billerica, MA). The concentrations of water-soluble inorganic ions,
183 including NO₃⁻, SO₄²⁻, Cl⁻, Ca²⁺, Mg²⁺, Na⁺, and NH₄⁺ in the samples were determined
184 using an ion chromatograph system (Dionex Aquion, Thermo Scientific, USA) (Xu et
185 al., 2022a; Lin et al., 2023).

186

187 **2.3. Compound categorization and predictions of ALW, pH, and hydroxyl radical**

188 The molecular formulas identified by UPLC-ESI-QToFMS were classified into
189 several major compound classes based on their elemental compositions (i.e., C, H, O,
190 and N), primarily including CHO, CHON, and CHN groups in the ESI+ mode and CHO
191 and CHON groups in the ESI- mode (Wang et al., 2017b). Unless stated otherwise, all
192 of the detected molecules were reported as neutral molecules. The double-bond
193 equivalent (DBE) and carbon oxidation state (OS_C) were calculated to reflect the
194 unsaturation degree of the organics and the composition evolution of organics that
195 underwent oxidation processes, respectively (details in **Sect. S2**) (Kroll et al., 2011; Xu
196 et al., 2023). Additionally, the modified aromaticity index (AI_{mod}) was also calculated
197 to indicate the aromaticity of organic compounds (details in **Sect. S2**) (Koch and
198 Dittmar, 2006).

199 A thermodynamic model (ISORROPIA-II) was applied to predict the mass
200 concentration of aerosol liquid water (ALW) and the value of pH with particle-phase

201 ion concentrations as well as ambient temperature and relative humidity as the inputs,
202 as detailed in our previous publications (Xu et al., 2020; Xu et al., 2023; Xu et al.,
203 2022b). The model output results based on our data set showed that 94% and 90% of
204 NO_3^- were in the aerosol phase in the cold and warm periods, respectively. Hence, the
205 predictions of pH and ALW were conducted without considering gaseous nitric acid
206 (Guo et al., 2015; Wang et al., 2021c). 78% and 21% of NH_4^+ were in the aerosol phase
207 in the cold and warm periods, respectively. Moreover, it is important to note that
208 gaseous NH_3 measurements were not conducted and ammonia partitioning was not
209 considered in this study. Thus, a bias correction of 1 pH unit was applied to calculate
210 the aerosol pH values (Guo et al., 2015; Wang et al., 2021c). The concentrations of
211 ambient $\bullet\text{OH}$ were predicted using empirical formula (Ehhalt and Rohrer, 2000; Wang
212 et al., 2020).

213

214 **3. Results and discussion**

215 **3.1. Overall molecular characterization of organic aerosols**

216 **Figures 1a** and **1c** show the mass spectra of organic compounds detected in ESI+
217 and ESI-, respectively. More compounds were identified in ESI+ (1885 molecular
218 formulas) than in ESI- (438 molecular formulas) (**Table S2**), which was similar to
219 previous reports about the molecular characteristic of biomass burning aerosols and
220 urban aerosols (Jiang et al., 2022; Wang et al., 2017b). The molecular weights of the
221 compounds with relatively high signal intensity mainly ranged from 100 Da to 500 Da
222 in ESI+, which was larger than those (100–300 Da) observed in the urban (Changchun,

223 Guangzhou, and Shanghai) (Wang et al., 2021a) and agriculture (Suixi) (Wang et al.,
224 2017b) regions of China. In contrast, the species with the strong signal intensity fell
225 between 100 Da and 300 Da in ESI⁻. This mass range detected in Urumqi organic
226 aerosols was comparable to previous observations in urban (Xi'an) aerosols (Han et
227 al., 2023) but significantly lower than that in firework-related urban (Beijing) aerosols
228 (300–400 Da) (Xie et al., 2020). On average, the molecular number and relative
229 abundance of CHON compounds (150–500 Da) were dominant in ESI⁺, accounting
230 for 45.99% of the total molecular number and $62.70 \pm 6.83\%$ of the total signal
231 intensity (**Figures 1a** and **Table S2**). CHO compounds were the second most abundant
232 categories ($28.76 \pm 4.75\%$ of the total signal intensity), followed by CHN compounds.
233 However, previous observations conducted in Shanghai, Guangzhou, and Changchun
234 suggested that the compounds in ESI⁺ were dominated by CHN and CHON species
235 (Wang et al., 2021a). In ESI⁻, although the number of CHON compounds was less
236 than CHO, the relative abundance of CHON compounds (150–250 Da) was higher
237 (**Figures 1d** and **Table S2**). The finding was consistent with the results obtained in
238 Shanghai and Changchun but different from the case in Guangzhou (Wang et al.,
239 2021a). The average H/C ratios of CHO (1.62–1.66) and CHON (1.79–1.83)
240 compounds in ESI⁺ mode (**Table S3**) were higher than those (0.94–1.13 for CHO and
241 1.27–1.47 for CHON) in Changchun, Shanghai, and Guangzhou (Wang et al., 2021a).
242 However, the average O/C ratios of CHO (0.25–0.3) and CHON (0.22–0.3)
243 compounds in ESI⁺ mode (**Table S3**) were less than those (0.42–0.43 for CHO and
244 0.27–0.45 for CHON) in the urban areas (Shanghai and Guangzhou) (Wang et al.,

245 2021a). Overall, these dissimilarities in molecular characteristics of organic aerosols
246 between Urumqi and other areas may be attributed to their different sources and
247 formation mechanisms.

248 **Figures 1b** and **1d** show the time series of the fractional distributions of various
249 organic matter categories in different ion modes. The abundance of CHO compounds
250 in ESI+ exhibited a temporal variation similar to that of CHON compounds ($r = 0.51$,
251 $P < 0.01$), with increased levels in the warm period. This indicated that CHO
252 compounds may be important precursors for the formation of NOCs (via reactions in
253 the gas- and/or particle-phases) or that they have similar origins. Previous simulation
254 experiments have demonstrated that higher temperatures increase the concentration of
255 oxygenated organic molecules, while lower temperatures can allow less oxidized
256 species to condense (Stolzenburg et al., 2018; Frege et al., 2018). In addition, solar
257 radiation and atmospheric oxidation capacity are also important factors promoting the
258 formation of more oxygenated organic molecules (Li et al., 2022; Liu et al., 2022). Air
259 temperature, radiation, and atmospheric oxidation capacity were much higher in the
260 warm period than in the cold period in Urumqi (**Table S1**) (Wan et al., 2021), which
261 may be partly responsible for increased abundances of CHO and CHON compounds in
262 the warm period. However, the abundance of CHN compounds tended to increase from
263 the warm period to the cold period. Since the ESI+ mode is highly sensitive to
264 protonatable species, organic amines were expected to predominate the CHN
265 compounds (Han et al., 2023; Wang et al., 2021a). It is well documented that the
266 formation of amine salt in the particle phase is tightly associated with aerosol acidity

267 and water (Liu et al., 2023). Thus, the reduced pH value and increased ALW level in
268 the cold period (**Table S1**) provided greater potential for converting gaseous amines
269 into particles.

270 In ESI⁻ mode, the abundances of CHON and CHO compounds exhibited a
271 significantly increased level in the cold period (**Figure 1d**), a variation pattern which
272 was completely opposite to the case in ESI⁺ mode. The ESI⁻ mode is more sensitive
273 to deprotonatable compounds like nitrophenols, organic nitrates, organosulfates, and
274 organic acids (Jiang et al., 2022; Lin et al., 2012). The formations of these compounds
275 were highly impacted by ALW and aerosol acidity (Ma et al., 2021; Smith et al., 2014;
276 Zhou et al., 2023; Xu et al., 2023). However, Urumqi has dry and dusty weather,
277 particularly in warm period, resulting in a quite low ALW concentration (1.86 ± 1.90
278 $\mu\text{g m}^{-3}$) in the warm period (**Table S1**). Moreover, the calculated mean pH value was
279 6.86 ± 1.71 (**Table S1**) during the warm period, which implies that the fine aerosol
280 particles in the warm period in Urumqi was neutral or slightly alkaline. Obviously, the
281 aerosol characteristics of the warm period in Urumqi may hinder the formation of these
282 organic compounds measured in ESI⁻ mode. In contrast, the increased ALW
283 concentration and decreased pH value during the cold period can facilitate the
284 formation of CHO and CHON compounds through the partitioning of gas-phase species
285 to the particles and subsequent aqueous phase reactions (Xu et al., 2020; Xu et al., 2023).
286 Furthermore, the total signal intensity of CHO compounds was significantly correlated
287 with that of CHON ($r = 0.62$, $P < 0.01$), indicating that they may have similar origins
288 or that CHO compounds may serve as important precursors for CHON compound

289 formation. It should be noted that this study mainly focuses on NOCs, therefore sulfur-
290 containing species were not discussed. In general, the differentiated seasonal variation
291 patterns for the different types of NOCs measured here can be attributed to the unique
292 meteorological conditions in Urumqi and different ionization mechanisms in ESI+ and
293 ESI- modes. The sources and formation mechanisms of NOCs will be further discussed
294 in the following sections.

295

296 **3.2. Seasonally differential sources and formation mechanisms of CHON** 297 **compounds**

298 CHON compounds can be derived from the reactions between CHO species and
299 reactive nitrogen species (NO_x , NH_3 , and NH_4^+) (Lee et al., 2016; De Haan et al., 2017),
300 as also partly implied by significant positive correlations ($r = 0.51\text{--}0.62$, $P < 0.01$)
301 between total signal intensity of CHO and CHON compounds in both ESI+ and ESI-
302 modes. Thus, CHO compounds were further classified based on their OS_C values to
303 preliminarily explore their origins and linkages with CHON compound formation
304 (**Figures 2a** and **2b**). In ESI+ mode, the OS_C values of the detected CHO compounds
305 (-1.75 to 0.5) were higher than those of primary vehicle exhausts (-2.0 to -1.9) (Aiken
306 et al., 2008), likely indicating a weak (or indirect) contribution of primary vehicle
307 exhausts to CHO molecules in Urumqi. The signal intensity of BBOA dominated the
308 total OA signal intensity and was higher in the warm period than in the cold period
309 (**Figure 2e**). However, previous studies conducted in China (e.g., Beijing, Xi'an,
310 Shanghai, and Liaocheng) suggested that biomass burning was more significant in the

311 cold seasons (Li et al., 2023; Wang et al., 2017a; Chen et al., 2017; Wang et al., 2009;
312 Wang et al., 2018; Zhang et al., 2022). Furthermore, we found that the oxygen-poor
313 unsaturated aliphatic compounds showed a high signal intensity in the warm period and
314 that the signal intensities of all categories of compounds in the warm period were
315 weakly correlated with atmospheric oxidants (i.e., O₃ and •OH) ($r < 0.1$, $P > 0.05$).
316 Thus, the formation or source of CHO compounds in the warm period may not be
317 mainly controlled by high atmospheric oxidation but rather by biomass burning, which
318 was distinguished from previous reports (Duan et al., 2020; Kondo et al., 2007; Zhang
319 et al., 2023). This consideration was also supported by the fact that there were
320 significantly more fire spots in the warm period than in the cold period (**Figure 3**). It
321 should be noted that the materials used for biomass burning in the cold period in rural
322 China are typically old-age plant tissues, such as dead branches of pine trees, dead
323 branches of shrubs, corn straw, and rice straw (**Figure S3**), while biomass burning in
324 the warm season is mainly attributed to forest fires or wildfires (relatively fresh
325 biomass). Accordingly, a large number of fresh biomass material burning occurred from
326 April to October each year in the neighboring countries (e.g., Kazakhstan) (Xu et al.,
327 2021) or regions of Urumqi (due to drought) (**Figure 3**) may be largely responsible for
328 high CHO compound abundance in the warm period.

329 The CHO species in ESI⁻ had higher OS_C (-1.85 to 1.1) than those in ESI⁺ (-1.85
330 to 0.25) (**Figures 2c** and **2d**), which was consistent with a recent study conducted in
331 Guangzhou, China (Zou et al., 2023). The predominant subgroups of CHO in ESI⁻
332 were BBOA (66.4% of total signal intensity) and semivolatile oxidized OA (SV-OOA)

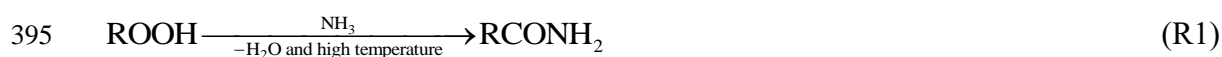
333 (23.1% of total signal intensity), which was different from the observation in Shanghai
334 (dominated by SV-OOA and low-volatility oxidized OA) (Wang et al., 2017a).
335 Additionally, some specific saturated and unsaturated aliphatic CHO substances (i.e.,
336 $C_{12-18}H_nO_2$) in ESI⁻ showed higher abundance in the warm season than in the cold
337 season, which was contrary to the variation pattern of other CHO compounds. These
338 $C_{12-18}H_nO_2$ compounds were found to be mainly fatty acids, such as stearic acid
339 ($C_{18}H_{36}O_2$), oleic acid ($C_{18}H_{34}O_2$), linoleic acid ($C_{18}H_{32}O_2$), palmitic acid
340 ($C_{16}H_{32}O_2$), and palmitoleic acid ($C_{16}H_{30}O_2$) (**Figure S4**), all of which usually
341 accumulate in plants, particularly *Suaeda aralocaspica* (W. Hogg and T. Gillan, 1984;
342 Wang et al., 2011). Interestingly, this plant was widely distributed in Central Asia as
343 well as on the southern edge of the Junggar Basin in Xinjiang, China (Wang et al., 2011).
344 Although fatty acids can also originate from food cooking (Zhao et al., 2007), there
345 seem to be no seasonal differences in cooking behavior locally. Thus, these results
346 further confirmed our consideration that the abundance of CHO compounds in the
347 warm period was highly impacted by fresh biomass material burning (e.g., forest fires
348 or wildfires).

349 CHON molecules in ESI⁺ were mainly identified as unsaturated aliphatic-like
350 compounds with poor oxygen (**Figures 4a** and **4b**), accounting for more than 70% of
351 the total signal intensities of CHON species (**Figure S5**). The signal intensity of CHON
352 species in ESI⁺ was greater in the warm period than in the cold period (**Figure 4e**).
353 Moreover, BBOA contributed to 56.9 % of the total CHON signal intensity in the warm
354 period (**Figure S6**). These characteristics of CHON compounds were similar to those

355 of CHO. Considering a significant positive correlation ($r = 0.62$, $P < 0.01$) between the
356 total signal intensity of CHO and CHON compounds in ESI+, we thus concluded that
357 primary sources (i.e., fresh biomass material burning) were also one of the main sources
358 of CHON compounds. In this study, CHON compounds with $O/N < 3$ contributed 76.48
359 $\pm 1.11\%$ of total CHON species in ESI+ (**Figure S7**), which was much larger than the
360 results observed in urban Tianjin in winter (less than 20%) (Zhong et al., 2023). In
361 particular, $C_{16}H_{33}ON$, $C_{18}H_{37}ON$, $C_{18}H_{35}ON$, $C_{18}H_{33}ON$, $C_{18}H_{31}ON$, and $C_{20}H_{33}ON$
362 showed a high abundance, together accounting for $55.04 \pm 7.09\%$ of the total CHON
363 abundance (**Table S4**). The carbon number of these compounds was consistent with
364 that of fatty acids mentioned above; moreover, their abundances showed a positive
365 correlation ($r = 0.43\text{--}0.81$, $P < 0.01$) with the abundances of corresponding fatty acids
366 in the warm period. In contrast, these CHON compounds only showed a weak
367 correlation ($r = -0.24 \sim 0.33$) with atmospheric oxidants (e.g., $\bullet OH$, O_3 , and NO_x). Thus,
368 the formation mechanism of biomass burning-related NOCs in Urumqi during the warm
369 period may be the interaction between fatty acids and reduced nitrogen species (e.g.,
370 NH_3) rather than the oxidation pathway involving CHO compounds and NO_x .

371 A recent laboratory study has suggested that NH_3 produced during the thermal
372 degradation of amino acids can react with oleic acid from the pyrolysis of triglycerides
373 to form amides (R1) (Ditto et al., 2022a). As discussed above, the combustion of fresh
374 biomass materials (e.g., forest fires or wildfires) can release abundant fatty acids. In
375 addition, wildfires can also emit large amounts of NH_3 , with an average emission factor
376 more than twice the NH_3 emission factor of agricultural fires (Tomsche et al., 2023).

377 According to MS/MS analysis (**Table S5**), potential fatty acid-derived NOCs were
 378 indeed identified as amides. Thus, we proposed that the high temperature generated
 379 during wildfires or forest fires provides suitable conditions for the reaction of
 380 carboxylic acids and NH₃ to form amides. The specific process was presented in **Figure**
 381 **5** (Pathway 1). It has been suggested that atmospheric oxidants can oxidize olefins (R2
 382 and R3) to form hydroxyl nitrates and carbonyl nitrates (Perring et al., 2013). Therefore,
 383 fatty acids (oleic acid as a representative) released from fresh biomass material burning
 384 may also rely on oxidation pathways to form NOCs (**Figure 5**, Pathway 2). It is worth
 385 noting that some products with double bonds after the amidation of unsaturated fatty
 386 acids can continue to undergo the reactions of R2 and R3 in the atmosphere, resulting
 387 in the formation of nitrooxy amides (**Figure 5**, Pathway 3). However, we found that the
 388 abundance of oleic acid-derived amides via Pathway 1 in the warm period was more
 389 than 100 times higher than that of NOCs with –ONH₂ (thus, the impact of ionization
 390 efficiency is expected to be less than 100 times) from Pathways 3. In the cold period,
 391 the abundance of fatty acids-derived amides decreased dramatically (**Figure 5** and
 392 **Figure S8**). Thus, the overall results demonstrated that the combustion of fresh biomass
 393 materials indeed contributed significantly to aerosol NOCs (e.g., amides) in the warm
 394 period in Urumqi.



398 The CHON species detected in ESI⁻ were mainly aromatic-like compounds,
399 whose signal intensities were significantly greater in the cold period than in the warm
400 period (**Figures 4c,4e** and **Figure S5**). Moreover, we found that several nitro-aromatic
401 compounds, including C₆H₅O₃N, C₆H₅O₄N, C₇H₇O₃N, C₇H₇O₄N, C₇H₅O₅N, and
402 C₈H₉O₃N (confirmed by their authentic standards in the LC/MS analysis), contributed
403 up to 50% of the total CHON (ESI⁻ mode) intensity (**Table S6**). Other NOCs with
404 relatively high signal intensity were mainly O₄₋₆N₂ species (contributed up to 25%),
405 such as C₆H₄O₅N₂, C₇H₄O₇N₂, C₇H₆O₅N₂, and C₇H₆O₆N₂, which have been suggested
406 to be associated with secondary photochemical or multiphase chemical processes
407 (Harrison et al., 2005; Cecinato et al., 2005; Salvador et al., 2021). However, the
408 abovementioned nitro-aromatic compounds including C₆H₅O₃N (nitrophenol),
409 C₆H₅O₄N (nitrocatechol), C₇H₇O₃N (methyl-nitrophenol), and C₇H₇O₄N (methyl-
410 nitrocatechol) were primarily identified as tracers of straw and wood burning (old-age
411 biomass materials commonly used in suburban and rural China) (Iinuma et al., 2010;
412 Kourtchev et al., 2016). A study about molecular characterization (ESI⁻ mode) of
413 water-soluble aerosols emitted from the combustion of old-age biomass materials (i.e.,
414 dry corn straw, rice straw, and pine branches) and coal showed that OA from old-age
415 biomass burning typically contained much more nitro compounds and/or organonitrates
416 than that from coal, while OA from coal-smoke contained more sulfur-containing
417 compounds (Song et al., 2018). Thus, the old-age biomass burning associated with
418 winter heating rather than coal combustion may contribute a significant amount of
419 aerosol NOCs (e.g., nitrophenols) in wintertime Urumqi. However, it does not

420 necessarily suggest that the importance of multiphase chemistry in the formation of
421 NOCs was ignorable, as indicated by relatively high signal intensity of O₄₋₆N₂ species.
422 In general, the differential molecular characteristics of CHON species in different
423 seasons in Urumqi can largely attributed to different impacts of the combustion of fresh-
424 and old-age biomass materials.

425

426 **3.3. CHN molecule evidence of fresh and old-age biomass burning in different** 427 **periods.**

428 **Figures 6a** and **6b** present the van Krevelen diagram of CHN compounds in the
429 cold and warm periods. The CHN₁ compounds with relatively high signal intensity
430 mainly contained 7–20 carbon atoms, among which C₅H₅N(CH₂)_n, C₉H₇N(CH₂)_n, and
431 C₁₃H₉N(CH₂)_n were dominant (78.68 ± 7.59 % of the total signal intensity of CHN₁
432 compounds in the cold period, **Table S7**). C₅H₅N(CH₂)_n could be identified as pyridine
433 and its homologues, which have been detected in freshly discharged BBOA (Dou et al.,
434 2015). Additionally, the abundance of C₅H₅N(CH₂)_n was positively correlated with that
435 of C₉H₇N(CH₂)_n, C₁₃H₉N(CH₂)_n, and nitro-aromatic compounds mentioned above ($r =$
436 0.46–0.81, $P < 0.01$), particularly in the cold period with old-age biomass burning for
437 heating. We further found that both the total signal intensity and aromaticity of CHN₁
438 species were much higher in the cold period (AI_{mod} of 0.52) than in the warm period
439 (AI_{mod} of 0.35) (**Figure 6** and **Figure S9**). It has been suggested that old-age leaves
440 contain more aromatic compounds compared to fresh leaves (Jian et al., 2016). Thus,
441 the overall results implied that old-age biomass burning had an important contribution

442 to the variation of CHN₁ compounds. In particular, the intensity of CHN₁ compounds
443 was significantly negatively correlated with the concentration of O₃ and •OH ($r = -0.44$
444 ~ -0.53 , $P < 0.01$), suggesting that atmospheric oxidation processes were the potential
445 pathway for amine removal rather than the sources of particle amine salts (Zahardis et
446 al., 2008; Qiu and Zhang, 2013). This result differed from the previous case, which
447 showed that the formation processes of CHN₁ and its homologs in Guangzhou (South
448 China) were tightly related to photo-oxidation processes (Jiang et al., 2022). The CHN₂
449 species showed a similar temporal variation pattern to the CHN₁ species. Moreover, the
450 abundances of total CHN₂ and major components (C₈₋₁₁H₈N₂(CH₂)_n, C₁₀H₁₄N₂(CH₂)_n,
451 C₁₀H₁₆N₂(CH₂)_n and C₅H₈N₂(CH₂)_n) were positively correlated with that of total CHN₁
452 ($r = 0.55-0.90$, $P < 0.01$), but negatively correlated with the concentration of O₃
453 and •OH ($r = -0.43 \sim -0.60$, $P < 0.01$). Clearly, old-age biomass burning, particularly
454 in the cold period, also exerted significant impacts on the abundance of CHN₂
455 compounds, which was also supported by several previous studies (Laskin et al., 2009;
456 Wang et al., 2017b; Song et al., 2022). A study about molecular characterization (ESI+
457 mode) of humic-like substances emitted from the combustion of old-age biomass
458 materials (i.e., dry corn straw, rice straw, and pine branches) and coals showed that OA
459 from old-age biomass burning typically contained much more CHN₂ compounds (55–
460 64%) than that from coal (20–37%), while OA from coal-smoke showed more CHN₁
461 compounds (78–84%) compared to that from old-age biomass materials (15–22%)
462 (Song et al., 2022). In this study, the signal intensity of CHN₁ compounds in the cold
463 period was about 40% higher than that in the warm period, while that of CHN₂

464 compounds showed a 160% increase from the warm period to the cold period. Thus,
465 although the contribution of fossil fuel (e.g., coal) combustion to NOCs in the cold
466 period cannot be ignored, our results at least suggested that the biomass burning-derived
467 CHN compounds showed a more significant increase compared to coal combustion-
468 derived compounds from the warm period to the cold period in Urumqi.

469 Interestingly, we found some CHN species with 16–20 carbon atoms showed
470 higher abundance in the warm period than in the cold period, a pattern opposite to that
471 of all other CNH compounds (**Figure 6c**). These $C_{16-20}N_1H_x$ compounds were further
472 identified as alkyl nitriles (**Table S5**) (Simoneit et al., 2003). In addition, the carbon
473 number of the identified alkyl nitriles was consistent with those of amides previously
474 proposed to be produced by fresh biomass burning. Thus, we proposed that fresh
475 biomass material burning in the warm period may provide a continuous high-
476 temperature environment to promote the dehydration of amides (**Figure 5**, Pathway 4).
477 These alkyl nitriles with double bonds can continue to undergo the reactions of R2 and
478 R3 (**Figure 5**, Pathway 5). However, the signal intensity of the nitrooxy products in the
479 warm period was insignificantly correlated with the concentration of O_3 , $\cdot OH$, and NO_x
480 ($P > 0.05$), likely indicating a weak influence of atmospheric oxidation on alkyl nitrile
481 removal in this site. The high-temperature dehydration of amides (e.g., erucamide) to
482 form alkyl nitriles (e.g., erucyl nitrile) has been demonstrated by Simoneit et al. (2003)
483 in a laboratory simulation experiment. A study on BBOA also showed that alkyl nitriles
484 can be serve as indicators of biomass burning in the ambient atmosphere (Radzi Bin
485 Abas et al., 2004). Furthermore, the abundance of identified alkyl nitriles initially

486 increased from March and peaked in September and October (**Figure S10**), a pattern
487 which was consistent with the interannual variation in wildfire areas (more in the warm
488 period) in Central Asian countries (Xu et al., 2021). Although cooking is also a potential
489 source of alkyl nitriles (Schauer et al., 1999), this activity does not have seasonal
490 differences. In contrast, the dramatically increased abundance of aromatic CNH
491 compounds in the cold period (**Figure S9**) can be attributed to the aqueous reactions of
492 amines emitted from old-age biomass material and coal combustion with acidic
493 substances, as indicated by significant correlations ($r = 0.61\text{--}0.95$, $P < 0.01$) between
494 total CHN abundance and SO_4^{2-} and NO_3^- concentrations. These findings further
495 confirmed that the NOCs from the combustion of fresh biomass materials in the warm
496 period in suburban Urumqi were compositionally different from those from old-age
497 biomass burning in the cold period.

498

499 **4. Conclusions**

500 The complexity of NOCs restricts our understanding of its sources and formation
501 processes. In this study, the molecular compositions of organic aerosols in $\text{PM}_{2.5}$
502 collected in Urumqi over a one-year period were systematically characterized in both
503 ESI⁻ and ESI⁺ modes, with a major focus on NOCs. A large amount of NOCs were
504 identified, showing that NOCs in relatively highly oxidative and reduced forms can be
505 roughly distinguished via these two ionization modes. Based on the identification of
506 molecular markers of amides and alkyl nitriles (much higher in the warm period) and
507 the analysis of their formation mechanisms (less contribution of atmospheric oxidation),

508 we highlighted the important contribution of combustion of fresh biomass materials
509 such as forest fires and wildfires to NOCs in the warm season in Urumqi. In contrast,
510 the dramatically increased abundances of aromatic CNH compounds and nitro-aromatic
511 CHON compounds (mainly nitrophenols) in the cold period were tightly associated
512 with the impacts of old-age biomass material burning. These results were illustrated in
513 a diagram (**Figure 7**).

514 Biomass materials in rural China were typically old-age plant tissues, as
515 mentioned above. Fresh biomass materials (e.g., green vegetation) with the enrichment
516 of oils and proteins can exist in forest fires or wildfires. Indeed, previous studies have
517 suggested that biomass burning can lead to the formation of aerosol amines and nitriles.
518 However, field observation studies have yet to pay attention to the differences in aerosol
519 NOCs emitted from the combustion of fresh and old-age biomass materials. For the
520 first time, our results reveal that fresh biomass material combustion can contribute more
521 amines and nitriles than old-age biomass material combustion. Generally, this study
522 provides field evidence on the differential impacts of the combustion of fresh and old-
523 age biomass materials on aerosol NOCs, improving our current understanding of the
524 molecular compositions of organic nitrogen aerosols in a vast territory with a sparse
525 population in Northwest China. Moreover, according to the fact that the studied site is
526 highly affected by combustion emissions of different types of biomass materials, future
527 work is needed to deeply understand the quantitative contributions of different types of
528 biomass burning to OA in China.

529

530 **Data availability.** The data in this study are available at
531 <https://doi.org/10.5281/zenodo.10453929>

532

533 **Competing interests.** The authors declare no conflicts of interest relevant to this study.

534

535 **Supplement.** Details of chemical analysis and data processing, eight tables (Tables
536 S1–S8), and ten extensive figures (Figures S1–S10).

537

538 **Author contributions.** YX designed the study. YJM, TY, and HWX performed field
539 measurements and sample collection; YJM and TY performed chemical analysis; YX
540 and YJM performed data analysis; YX and YJM wrote the original manuscript; and YX,
541 YJM, HWX, and HYY reviewed and edited the manuscript.

542

543 **Financial support.** This study was kindly supported by the National Natural Science
544 Foundation of China through grant 42303081 (Y. Xu) and Shanghai “Science and
545 Technology Innovation Action Plan” Shanghai Sailing Program through grant
546 22YF1418700 (Y. Xu).

547

548 **References**

549 Aiken, A. C., Decarlo, P. F., Kroll, J. H., Worsnop, D. R., Huffman, J. A., Docherty,
550 K. S., Ulbrich, I. M., Mohr, C., Kimmel, J. R., Sueper, D., Sun, Y., Zhang, Q., Trimborn,
551 A., Northway, M., Ziemann, P. J., Canagaratna, M. R., Onasch, T. B., Alfarra, M. R.,

552 Prevot, A. S., Dommen, J., Duplissy, J., Metzger, A., Baltensperger, U., and Jimenez, J.
553 L.: O/C and OM/OC ratios of primary, secondary, and ambient organic aerosols with
554 high-resolution time-of-flight aerosol mass spectrometry, *Environ. Sci. Technol.*, 42,
555 4478-4485, <https://doi.org/10.1021/es703009q>, 2008.

556 Altieri, K. E., Fawcett, S. E., Peters, A. J., Sigman, D. M., and Hastings, M. G.:
557 Marine biogenic source of atmospheric organic nitrogen in the subtropical North
558 Atlantic, *P. Natl. Acad. Sci. USA*, 113, 925-930,
559 <https://doi.org/10.1073/pnas.1516847113>, 2016.

560 Bandowe, B. A. M. and Meusel, H.: Nitrated polycyclic aromatic hydrocarbons
561 (nitro-PAHs) in the environment – A review, *Sci. Total Environ.*, 581-582, 237-257,
562 <https://doi.org/10.1016/j.scitotenv.2016.12.115>, 2017.

563 Bátori, Z., Erdős, L., Kelemen, A., Deák, B., Valkó, O., Gallé, R., Bragina, T. M.,
564 Kiss, P. J., Kröel-Dulay, G., and Tölgyesi, C.: Diversity patterns in sandy forest-steppes:
565 a comparative study from the western and central Palaeartic, *Biodivers. Conserv.*, 27,
566 1011-1030, <https://doi.org/10.1007/s10531-017-1477-7>, 2018.

567 Cape, J. N., Cornell, S. E., Jickells, T. D., and Nemitz, E.: Organic nitrogen in the
568 atmosphere — Where does it come from? A review of sources and methods, *Atmos.
569 Res.*, 102, 30-48, <https://doi.org/10.1016/j.atmosres.2011.07.009>, 2011.

570 Cecinato, A., Di Palo, V., Pomata, D., Tomasi Scianò, M. C., and Possanzini, M.:
571 Measurement of phase-distributed nitrophenols in Rome ambient air, *Chemosphere*, 59,
572 679-683, <https://doi.org/10.1016/j.chemosphere.2004.10.045>, 2005.

573 Chen, J., Li, C., Ristovski, Z., Milic, A., Gu, Y., Islam, M. S., Wang, S., Hao, J.,

574 Zhang, H., He, C., Guo, H., Fu, H., Miljevic, B., Morawska, L., Thai, P., Lam, Y. F.,
575 Pereira, G., Ding, A., Huang, X., and Dumka, U. C.: A review of biomass burning:
576 Emissions and impacts on air quality, health and climate in China, *Sci. Total Environ.*,
577 579, 1000-1034, <https://doi.org/10.1016/j.scitotenv.2016.11.025>, 2017.

578 De Haan, D. O., Hawkins, L. N., Welsh, H. G., Pednekar, R., Casar, J. R.,
579 Pennington, E. A., de Loera, A., Jimenez, N. G., Symons, M. A., Zauscher, M., Pajunoja,
580 A., Caponi, L., Cazaunau, M., Formenti, P., Gratien, A., Pangui, E., and Doussin, J.-F.:
581 Brown Carbon Production in Ammonium- or Amine-Containing Aerosol Particles by
582 Reactive Uptake of Methylglyoxal and Photolytic Cloud Cycling, *Environ. Sci.*
583 *Technol.*, 51, 7458-7466, <https://doi.org/10.1021/acs.est.7b00159>, 2017.

584 Ditto, J. C., Abbatt, J. P. D., and Chan, A. W. H.: Gas- and Particle-Phase Amide
585 Emissions from Cooking: Mechanisms and Air Quality Impacts, *Environ. Sci. Technol.*,
586 56, 7741-7750, <https://doi.org/10.1021/acs.est.2c01409>, 2022a.

587 Ditto, J. C., Machesky, J., and Gentner, D. R.: Analysis of reduced and oxidized
588 nitrogen-containing organic compounds at a coastal site in summer and winter, *Atmos.*
589 *Chem. Phys.*, 22, 3045-3065, <https://doi.org/10.5194/acp-22-3045-2022>, 2022b.

590 Ditto, J. C., Joo, T., Slade, J. H., Shepson, P. B., Ng, N. L., and Gentner, D. R.:
591 Nontargeted Tandem Mass Spectrometry Analysis Reveals Diversity and Variability in
592 Aerosol Functional Groups across Multiple Sites, Seasons, and Times of Day, *Environ.*
593 *Sci. Technol. Lett.*, 7, 60-69, <https://doi.org/10.1021/acs.estlett.9b00702>, 2020.

594 Dou, J., Lin, P., Kuang, B.-Y., and Yu, J. Z.: Reactive Oxygen Species Production
595 Mediated by Humic-like Substances in Atmospheric Aerosols: Enhancement Effects by

596 Pyridine, Imidazole, and Their Derivatives, *Environ. Sci. Technol.*, 49, 6457-6465,
597 <https://doi.org/10.1021/es5059378>, 2015.

598 Duan, J., Huang, R. J., Li, Y., Chen, Q., Zheng, Y., Chen, Y., Lin, C., Ni, H., Wang,
599 M., Ovadnevaite, J., Ceburnis, D., Chen, C., Worsnop, D. R., Hoffmann, T., O'Dowd,
600 C., and Cao, J.: Summertime and wintertime atmospheric processes of secondary
601 aerosol in Beijing, *Atmos. Chem. Phys.*, 20, 3793-3807, [https://doi.org/10.5194/acp-](https://doi.org/10.5194/acp-20-3793-2020)
602 [20-3793-2020](https://doi.org/10.5194/acp-20-3793-2020), 2020.

603 Ehhalt, D. H. and Rohrer, F.: Dependence of the OH concentration on solar UV, *J.*
604 *Geophys. Res.-Atmos.*, 105, 3565-3571, <https://doi.org/10.1029/1999JD901070>, 2000.

605 Franze, T., Weller, M. G., Niessner, R., and Pöschl, U.: Protein Nitration by
606 Polluted Air, *Environ. Sci. Technol.*, 39, 1673-1678, <https://doi.org/10.1021/es0488737>,
607 2005.

608 Frege, C., Ortega, I. K., Rissanen, M. P., Praplan, A. P., Steiner, G., Heinritzi, M.,
609 Ahonen, L., Amorim, A., Bernhammer, A. K., Bianchi, F., Brilke, S., Breitenlechner,
610 M., Dada, L., Dias, A., Duplissy, J., Ehrhart, S., El-Haddad, I., Fischer, L., Fuchs, C.,
611 Garmash, O., Gonin, M., Hansel, A., Hoyle, C. R., Jokinen, T., Junninen, H., Kirkby, J.,
612 Kürten, A., Lehtipalo, K., Leiminger, M., Mauldin, R. L., Molteni, U., Nichman, L.,
613 Petäjä, T., Sarnela, N., Schobesberger, S., Simon, M., Sipilä, M., Stolzenburg, D., Tomé,
614 A., Vogel, A. L., Wagner, A. C., Wagner, R., Xiao, M., Yan, C., Ye, P., Curtius, J.,
615 Donahue, N. M., Flagan, R. C., Kulmala, M., Worsnop, D. R., Winkler, P. M., Dommen,
616 J., and Baltensperger, U.: Influence of temperature on the molecular composition of
617 ions and charged clusters during pure biogenic nucleation, *Atmos. Chem. Phys.*, 18, 65-

618 79, <https://doi.org/10.5194/acp-18-65-2018>, 2018.

619 Guo, H., Xu, L., Bougiatioti, A., Cerully, K. M., Capps, S. L., Hite Jr, J. R., Carlton,
620 A. G., Lee, S. H., Bergin, M. H., Ng, N. L., Nenes, A., and Weber, R. J.: Fine-particle
621 water and pH in the southeastern United States, *Atmos. Chem. Phys.*, 15, 5211-5228,
622 <https://doi.org/10.5194/acp-15-5211-2015>, 2015.

623 Han, Y., Zhang, X., Li, L., Lin, Y., Zhu, C., Zhang, N., Wang, Q., and Cao, J.:
624 Enhanced Production of Organosulfur Species during a Severe Winter Haze Episode in
625 the Guanzhong Basin of Northwest China, *Environ. Sci. Technol.*,
626 <https://doi.org/10.1021/acs.est.3c02914>, 2023.

627 Harrison, M. A. J., Barra, S., Borghesi, D., Vione, D., Arsene, C., and Iulian Olariu,
628 R.: Nitrated phenols in the atmosphere: a review, *Atmos. Environ.*, 39, 231-248,
629 <https://doi.org/10.1016/j.atmosenv.2004.09.044>, 2005.

630 Iinuma, Y., Böge, O., Gräfe, R., and Herrmann, H.: Methyl-Nitrocatechols:
631 Atmospheric Tracer Compounds for Biomass Burning Secondary Organic Aerosols,
632 *Environ. Sci. Technol.*, 44, 8453-8459, <https://doi.org/10.1021/es102938a>, 2010.

633 Jian, Q., Boyer, T. H., Yang, X., Xia, B., and Yang, X.: Characteristics and DBP
634 formation of dissolved organic matter from leachates of fresh and aged leaf litter,
635 *Chemosphere*, 152, 335-344, <https://doi.org/10.1016/j.chemosphere.2016.02.107>, 2016.

636 Jiang, H., Li, J., Tang, J., Zhao, S., Chen, Y., Tian, C., Zhang, X., Jiang, B., Liao,
637 Y., and Zhang, G.: Factors Influencing the Molecular Compositions and Distributions
638 of Atmospheric Nitrogen-Containing Compounds, *J. Geophys. Res.-Atmos.*, 127,
639 e2021JD036284, <https://doi.org/10.1029/2021JD036284>, 2022.

640 Kenagy, H. S., Romer Present, P. S., Wooldridge, P. J., Nault, B. A., Campuzano-
641 Jost, P., Day, D. A., Jimenez, J. L., Zare, A., Pye, H. O. T., Yu, J., Song, C. H., Blake,
642 D. R., Woo, J.-H., Kim, Y., and Cohen, R. C.: Contribution of Organic Nitrates to
643 Organic Aerosol over South Korea during KORUS-AQ, *Environ. Sci. Technol.*, 55,
644 16326-16338, <https://doi.org/10.1021/acs.est.1c05521>, 2021.

645 Koch, B. P. and Dittmar, T.: From mass to structure: an aromaticity index for high-
646 resolution mass data of natural organic matter, *Rapid Commun. Mass Spectrom.*, 20,
647 926-932, <https://doi.org/10.1002/rcm.2386>, 2006.

648 Kondo, Y., Miyazaki, Y., Takegawa, N., Miyakawa, T., Weber, R. J., Jimenez, J.
649 L., Zhang, Q., and Worsnop, D. R.: Oxygenated and water-soluble organic aerosols in
650 Tokyo, *J. Geophys. Res.-Atmos.*, 112, <https://doi.org/10.1029/2006JD007056>, 2007.

651 Kourtchev, I., Godoi, R. H. M., Connors, S., Levine, J. G., Archibald, A. T., Godoi,
652 A. F. L., Paralovo, S. L., Barbosa, C. G. G., Souza, R. A. F., Manzi, A. O., Seco, R.,
653 Sjostedt, S., Park, J. H., Guenther, A., Kim, S., Smith, J., Martin, S. T., and Kalberer,
654 M.: Molecular composition of organic aerosols in central Amazonia: an ultra-high-
655 resolution mass spectrometry study, *Atmos. Chem. Phys.*, 16, 11899-11913,
656 <https://doi.org/10.5194/acp-16-11899-2016>, 2016.

657 Kroll, J. H., Donahue, N. M., Jimenez, J. L., Kessler, S. H., Canagaratna, M. R.,
658 Wilson, K. R., Altieri, K. E., Mazzoleni, L. R., Wozniak, A. S., Bluhm, H., Mysak, E.
659 R., Smith, J. D., Kolb, C. E., and Worsnop, D. R.: Carbon oxidation state as a metric
660 for describing the chemistry of atmospheric organic aerosol, *Nat. Chem.*, 3, 133-139,
661 <https://doi.org/10.1038/nchem.948>, 2011.

662 Laskin, A., Smith, J. S., and Laskin, J.: Molecular Characterization of Nitrogen-
663 Containing Organic Compounds in Biomass Burning Aerosols Using High-Resolution
664 Mass Spectrometry, *Environ. Sci. Technol.*, 43, 3764-3771,
665 <https://doi.org/10.1021/es803456n>, 2009.

666 Laskin, J., Laskin, A., Nizkorodov, S. A., Roach, P., Eckert, P., Gilles, M. K., Wang,
667 B., Lee, H. J., and Hu, Q.: Molecular Selectivity of Brown Carbon Chromophores,
668 *Environ. Sci. Technol.*, 48, 12047-12055, <https://doi.org/10.1021/es503432r>, 2014.

669 Lee, B. H., Mohr, C., Lopez-Hilfiker, F. D., Lutz, A., Hallquist, M., Lee, L., Romer,
670 P., Cohen, R. C., Iyer, S., Kurtén, T., Hu, W., Day, D. A., Campuzano-Jost, P., Jimenez,
671 J. L., Xu, L., Ng, N. L., Guo, H., Weber, R. J., Wild, R. J., Brown, S. S., Koss, A., de
672 Gouw, J., Olson, K., Goldstein, A. H., Seco, R., Kim, S., McAvey, K., Shepson, P. B.,
673 Starn, T., Baumann, K., Edgerton, E. S., Liu, J., Shilling, J. E., Miller, D. O., Brune, W.,
674 Schobesberger, S., D'Ambro, E. L., and Thornton, J. A.: Highly functionalized organic
675 nitrates in the southeast United States: Contribution to secondary organic aerosol and
676 reactive nitrogen budgets, *P. Natl. Acad. Sci. USA*, 113, 1516-1521,
677 <https://doi.org/10.1073/pnas.1508108113>, 2016.

678 Li, S., Liu, D., Kong, S., Wu, Y., Hu, K., Zheng, H., Cheng, Y., Zheng, S., Jiang,
679 X., Ding, S., Hu, D., Liu, Q., Tian, P., Zhao, D., and Sheng, J.: Evolution of source
680 attributed organic aerosols and gases in a megacity of central China, *Atmos. Chem.*
681 *Phys.*, 22, 6937-6951, <https://doi.org/10.5194/acp-22-6937-2022>, 2022.

682 Li, Y., Chen, M., Wang, Y., Huang, T., Wang, G., Li, Z., Li, J., Meng, J., and Hou,
683 Z.: Seasonal characteristics and provenance of organic aerosols in the urban atmosphere

684 of Liaocheng in the North China Plain: Significant effect of biomass burning,
685 *Particuology*, 75, 185-198, <https://doi.org/10.1016/j.partic.2022.07.012>, 2023.

686 Lin, P., Rincon, A. G., Kalberer, M., and Yu, J. Z.: Elemental Composition of
687 HULIS in the Pearl River Delta Region, China: Results Inferred from Positive and
688 Negative Electrospray High Resolution Mass Spectrometric Data, *Environ. Sci.*
689 *Technol.*, 46, 7454-7462, <https://doi.org/10.1021/es300285d>, 2012.

690 Lin, X., Xu, Y., Zhu, R.-G., Xiao, H.-W., and Xiao, H.-Y.: Proteinaceous Matter in
691 PM_{2.5} in Suburban Guiyang, Southwestern China: Decreased Importance in Long-
692 Range Transport and Atmospheric Degradation, *J. Geophys. Res.-Atmos.*, 128,
693 e2023JD038516, <https://doi.org/10.1029/2023JD038516>, 2023.

694 Liu, T., Xu, Y., Sun, Q.-B., Xiao, H.-W., Zhu, R.-G., Li, C.-X., Li, Z.-Y., Zhang,
695 K.-Q., Sun, C.-X., and Xiao, H.-Y.: Characteristics, Origins, and Atmospheric
696 Processes of Amines in Fine Aerosol Particles in Winter in China, *J. Geophys. Res.-*
697 *Atmos.*, 128, e2023JD038974, <https://doi.org/10.1029/2023JD038974>, 2023.

698 Liu, T., Hong, Y., Li, M., Xu, L., Chen, J., Bian, Y., Yang, C., Dan, Y., Zhang, Y.,
699 Xue, L., Zhao, M., Huang, Z., and Wang, H.: Atmospheric oxidation capacity and ozone
700 pollution mechanism in a coastal city of southeastern China: analysis of a typical
701 photochemical episode by an observation-based model, *Atmos. Chem. Phys.*, 22, 2173-
702 2190, <https://doi.org/10.5194/acp-22-2173-2022>, 2022.

703 Luo, Y., Zeng, Y., Xu, H., Li, D., Zhang, T., Lei, Y., Huang, S., and Shen, Z.:
704 Connecting oxidative potential with organic carbon molecule composition and source-
705 specific apportionment in PM_{2.5} in Xi'an, China, *Atmos. Environ.*, 306, 119808,

706 <https://doi.org/10.1016/j.atmosenv.2023.119808>, 2023.

707 Ma, L., Guzman, C., Niedek, C., Tran, T., Zhang, Q., and Anastasio, C.: Kinetics
708 and Mass Yields of Aqueous Secondary Organic Aerosol from Highly Substituted
709 Phenols Reacting with a Triplet Excited State, *Environ. Sci. Technol.*, *55*, 5772-5781,
710 <https://doi.org/10.1021/acs.est.1c00575>, 2021.

711 Nguyen, T. B., Bates, K. H., Crouse, J. D., Schwantes, R. H., Zhang, X.,
712 Kjaergaard, H. G., Surratt, J. D., Lin, P., Laskin, A., Seinfeld, J. H., and Wennberg, P.
713 O.: Mechanism of the hydroxyl radical oxidation of methacryloyl peroxyxynitrate (MPAN)
714 and its pathway toward secondary organic aerosol formation in the atmosphere, *Phys.*
715 *Chem. Chem. Phys.*, *17*, 17914-17926, <https://doi.org/10.1039/C5CP02001H>, 2015.

716 Perring, A. E., Pusede, S. E., and Cohen, R. C.: An Observational Perspective on
717 the Atmospheric Impacts of Alkyl and Multifunctional Nitrates on Ozone and
718 Secondary Organic Aerosol, *Chem. Rev.*, *113*, 5848-5870,
719 <https://doi.org/10.1021/cr300520x>, 2013.

720 Qiu, C. and Zhang, R.: Multiphase chemistry of atmospheric amines, *Phys. Chem.*
721 *Chem. Phys.*, *15*, 5738-5752, <https://doi.org/10.1039/C3CP43446j>, 2013.

722 Qizhi, M., Ying, L., Kang, W., and Qingfei, Z.: Spatio-Temporal Changes of
723 Population Density and Urbanization Pattern in China(2000–2010), *China City Plan.*
724 *Rev.*, *25*, 8-14, 2016.

725 Radzi Bin Abas, M., Rahman, N. A., Omar, N. Y. M. J., Maah, M. J., Abu Samah,
726 A., Oros, D. R., Otto, A., and Simoneit, B. R. T.: Organic composition of aerosol
727 particulate matter during a haze episode in Kuala Lumpur, Malaysia, *Atmos. Environ.*,

728 38, 4223-4241, <https://doi.org/10.1016/j.atmosenv.2004.01.048>, 2004.

729 Ren, Y., Wang, G., Wu, C., Wang, J., Li, J., Zhang, L., Han, Y., Liu, L., Cao, C.,
730 Cao, J., He, Q., and Liu, X.: Changes in concentration, composition and source
731 contribution of atmospheric organic aerosols by shifting coal to natural gas in Urumqi,
732 *Atmos. Environ.*, 148, 306-315, <https://doi.org/10.1016/j.atmosenv.2016.10.053>, 2017.

733 Rollins, A. W., Browne, E. C., Min, K.-E., Pusede, S. E., Wooldridge, P. J., Gentner,
734 D. R., Goldstein, A. H., Liu, S., Day, D. A., Russell, L. M., and Cohen, R. C.: Evidence
735 for NO_x Control over Nighttime SOA Formation, *Science*, 337, 1210-1212,
736 <https://doi.org/10.1126/science.1221520>, 2012.

737 Salvador, C. M. G., Tang, R., Priestley, M., Li, L., Tsiligiannis, E., Le Breton, M.,
738 Zhu, W., Zeng, L., Wang, H., Yu, Y., Hu, M., Guo, S., and Hallquist, M.: Ambient nitro-
739 aromatic compounds – biomass burning versus secondary formation in rural China,
740 *Atmos. Chem. Phys.*, 21, 1389-1406, <https://doi.org/10.5194/acp-21-1389-2021>, 2021.

741 Samy, S. and Hays, M. D.: Quantitative LC–MS for water-soluble heterocyclic
742 amines in fine aerosols (PM_{2.5}) at Duke Forest, USA, *Atmos. Environ.*, 72, 77-80,
743 <https://doi.org/10.1016/j.atmosenv.2013.02.032>, 2013.

744 Schauer, J. J., Kleeman, M. J., Cass, G. R., and Simoneit, B. R. T.: Measurement
745 of Emissions from Air Pollution Sources. 1. C₁ through C₂₉ Organic Compounds from
746 Meat Charbroiling, *Environ. Sci. Technol.*, 33, 1566-1577,
747 <https://doi.org/10.1021/es980076j>, 1999.

748 Seinfeld, J. H., Bretherton, C., Carslaw, K. S., Coe, H., DeMott, P. J., Dunlea, E.
749 J., Feingold, G., Ghan, S., Guenther, A. B., Kahn, R., Kraucunas, I., Kreidenweis, S.

750 M., Molina, M. J., Nenes, A., Penner, J. E., Prather, K. A., Ramanathan, V., Ramaswamy,
751 V., Rasch, P. J., Ravishankara, A. R., Rosenfeld, D., Stephens, G., and Wood, R.:
752 Improving our fundamental understanding of the role of aerosol–cloud interactions in
753 the climate system, *P. Natl. Acad. Sci. USA*, 113, 5781-5790,
754 <https://doi.org/10.1073/pnas.1514043113>, 2016.

755 Simoneit, B. R. T., Rushdi, A. I., bin Abas, M. R., and Didyk, B. M.: Alkyl Amides
756 and Nitriles as Novel Tracers for Biomass Burning, *Environ. Sci. Technol.*, 37, 16-21,
757 <https://doi.org/10.1021/es020811y>, 2003.

758 Smith, J. D., Sio, V., Yu, L., Zhang, Q., and Anastasio, C.: Secondary Organic
759 Aerosol Production from Aqueous Reactions of Atmospheric Phenols with an Organic
760 Triplet Excited State, *Environ. Sci. Technol.*, 48, 1049-1057,
761 <https://doi.org/10.1021/es4045715>, 2014.

762 Song, J., Li, M., Jiang, B., Wei, S., Fan, X., and Peng, P. a.: Molecular
763 Characterization of Water-Soluble Humic like Substances in Smoke Particles Emitted
764 from Combustion of Biomass Materials and Coal Using Ultrahigh-Resolution
765 Electrospray Ionization Fourier Transform Ion Cyclotron Resonance Mass
766 Spectrometry, *Environ. Sci. Technol.*, 52, 2575-2585,
767 <https://doi.org/10.1021/acs.est.7b06126>, 2018.

768 Song, J., Li, M., Zou, C., Cao, T., Fan, X., Jiang, B., Yu, Z., Jia, W., and Peng, P.
769 a.: Molecular Characterization of Nitrogen-Containing Compounds in Humic-like
770 Substances Emitted from Biomass Burning and Coal Combustion, *Environ. Sci.*
771 *Technol.*, 56, 119-130, <https://doi.org/10.1021/acs.est.1c04451>, 2022.

772 Stolzenburg, D., Fischer, L., Vogel, A. L., Heinritzi, M., Schervish, M., Simon, M.,
773 Wagner, A. C., Dada, L., Ahonen, L. R., Amorim, A., Baccharini, A., Bauer, P. S.,
774 Baumgartner, B., Bergen, A., Bianchi, F., Breitenlechner, M., Brilke, S., Buenrostro
775 Mazon, S., Chen, D., Dias, A., Draper, D. C., Duplissy, J., El Haddad, I., Finkenzeller,
776 H., Frege, C., Fuchs, C., Garmash, O., Gordon, H., He, X., Helm, J., Hofbauer, V.,
777 Hoyle, C. R., Kim, C., Kirkby, J., Kontkanen, J., Kürten, A., Lampilahti, J., Lawler, M.,
778 Lehtipalo, K., Leiminger, M., Mai, H., Mathot, S., Mentler, B., Molteni, U., Nie, W.,
779 Nieminen, T., Nowak, J. B., Ojdanic, A., Onnela, A., Passananti, M., Petäjä, T.,
780 Quéléver, L. L. J., Rissanen, M. P., Sarnela, N., Schallhart, S., Tauber, C., Tomé, A.,
781 Wagner, R., Wang, M., Weitz, L., Wimmer, D., Xiao, M., Yan, C., Ye, P., Zha, Q.,
782 Baltensperger, U., Curtius, J., Dommen, J., Flagan, R. C., Kulmala, M., Smith, J. N.,
783 Worsnop, D. R., Hansel, A., Donahue, N. M., and Winkler, P. M.: Rapid growth of
784 organic aerosol nanoparticles over a wide tropospheric temperature range, *P. Natl. Acad.*
785 *Sci. USA*, 115, 9122-9127, <https://doi.org/10.1073/pnas.1807604115>, 2018.

786 Surratt, J. D., Chan, A. W. H., Eddingsaas, N. C., Chan, M., Loza, C. L., Kwan, A.
787 J., Hersey, S. P., Flagan, R. C., Wennberg, P. O., and Seinfeld, J. H.: Reactive
788 intermediates revealed in secondary organic aerosol formation from isoprene, *P. Natl.*
789 *Acad. Sci. USA*, 107, 6640-6645, <https://doi.org/10.1073/pnas.0911114107>, 2010.

790 Tomsche, L., Piel, F., Mikoviny, T., Nielsen, C. J., Guo, H., Campuzano-Jost, P.,
791 Nault, B. A., Schueneman, M. K., Jimenez, J. L., Halliday, H., Diskin, G., DiGangi, J.
792 P., Nowak, J. B., Wiggins, E. B., Gargulinski, E., Soja, A. J., and Wisthaler, A.:
793 Measurement report: Emission factors of NH₃ and NH_x for wildfires and agricultural

794 fires in the United States, *Atmos. Chem. Phys.*, 23, 2331-2343,
795 <https://doi.org/10.5194/acp-23-2331-2023>, 2023.

796 W. Hogg, R. and T. Gillan, F.: Fatty acids, sterols and hydrocarbons in the leaves
797 from eleven species of mangrove, *Phytochemistry*, 23, 93-97,
798 [https://doi.org/10.1016/0031-9422\(84\)83084-8](https://doi.org/10.1016/0031-9422(84)83084-8), 1984.

799 Wan, X., Qin, F., Cui, F., Chen, W., Ding, H., and Li, C.: Correlation between the
800 distribution of solar energy resources and the cloud cover in Xinjiang, *IOP Conf. Ser.:*
801 *Earth Environ. Sci.*, 675, 012060, <https://doi.org/10.1088/1755-1315/675/1/012060>,
802 2021.

803 Wang, H., Wang, Q., Gao, Y., Zhou, M., Jing, S., Qiao, L., Yuan, B., Huang, D.,
804 Huang, C., Lou, S., Yan, R., de Gouw, J. A., Zhang, X., Chen, J., Chen, C., Tao, S., An,
805 J., and Li, Y.: Estimation of Secondary Organic Aerosol Formation During a
806 Photochemical Smog Episode in Shanghai, China, *J. Geophys. Res.-Atmos.*, 125,
807 e2019JD032033, <https://doi.org/10.1029/2019JD032033>, 2020.

808 Wang, K., Huang, R.-J., Brueggemand, M., Zhang, Y., Yang, L., Ni, H., Guo, J.,
809 Wang, M., Han, J., Bilde, M., Glasius, M., and Hoffmann, T.: Urban organic aerosol
810 composition in eastern China differs from north to south: molecular insight from a
811 liquid chromatography-mass spectrometry (Orbitrap) study, *Atmos. Chem. Phys.*, 21,
812 9089-9104, <https://doi.org/10.5194/acp-21-9089-2021>, 2021a.

813 Wang, L., Zhang, K., Huang, W., Han, W., and Tian, C.-Y.: Seed oil content and
814 fatty acid composition of annual halophyte *Suaeda acuminata*: A comparative study on
815 dimorphic seeds, *Afr. J. Biotechnol.*, 10, 19106-19108,

816 <https://doi.org/10.5897/ajb11.2597>, 2011.

817 Wang, Q., Shao, M., Zhang, Y., Wei, Y., Hu, M., and Guo, S.: Source
818 apportionment of fine organic aerosols in Beijing, *Atmos. Chem. Phys.*, 9, 8573-8585,
819 <https://doi.org/10.5194/acp-9-8573-2009>, 2009.

820 Wang, X., Hayeck, N., Brüggemann, M., Yao, L., Chen, H., Zhang, C., Emmelin,
821 C., Chen, J., George, C., and Wang, L.: Chemical Characteristics of Organic Aerosols
822 in Shanghai: A Study by Ultrahigh-Performance Liquid Chromatography Coupled With
823 Orbitrap Mass Spectrometry, *J. Geophys. Res.-Atmos.*, 122, 11,703-711,722,
824 <https://doi.org/10.1002/2017JD026930>, 2017a.

825 Wang, X., Shen, Z., Liu, F., Lu, D., Tao, J., Lei, Y., Zhang, Q., Zeng, Y., Xu, H.,
826 Wu, Y., Zhang, R., and Cao, J.: Saccharides in summer and winter PM_{2.5} over Xi'an,
827 Northwestern China: Sources, and yearly variations of biomass burning contribution to
828 PM_{2.5}, *Atmos. Res.*, 214, 410-417, <https://doi.org/10.1016/j.atmosres.2018.08.024>,
829 2018.

830 Wang, Y., Zhao, Y., Li, Z., Li, C., Yan, N., and Xiao, H.: Importance of Hydroxyl
831 Radical Chemistry in Isoprene Suppression of Particle Formation from α -Pinene
832 Ozonolysis, *ACS Earth Space Chem.*, 5, 487-499,
833 <https://doi.org/10.1021/acsearthspacechem.0c00294>, 2021b.

834 Wang, Y., Hu, M., Lin, P., Guo, Q., Wu, Z., Li, M., Zeng, L., Song, Y., Zeng, L.,
835 Wu, Y., Guo, S., Huang, X., and He, L.: Molecular Characterization of Nitrogen-
836 Containing Organic Compounds in Humic-like Substances Emitted from Straw
837 Residue Burning, *Environ. Sci. Technol.*, 51, 5951-5961,

838 <https://doi.org/10.1021/acs.est.7b00248>, 2017b.

839 Wang, Y., Hu, M., Hu, W., Zheng, J., Niu, H., Fang, X., Xu, N., Wu, Z., Guo, S.,
840 Wu, Y., Chen, W., Lu, S., Shao, M., Xie, S., Luo, B., and Zhang, Y.: Secondary
841 Formation of Aerosols Under Typical High-Humidity Conditions in Wintertime
842 Sichuan Basin, China: A Contrast to the North China Plain, *J. Geophys. Res.-Atmos.*,
843 126, e2021JD034560, <https://doi.org/10.1029/2021JD034560>, 2021c.

844 Xie, Q., Su, S., Chen, S., Xu, Y., Cao, D., Chen, J., Ren, L., Yue, S., Zhao, W., Sun,
845 Y., Wang, Z., Tong, H., Su, H., Cheng, Y., Kawamura, K., Jiang, G., Liu, C. Q., and Fu,
846 P.: Molecular characterization of firework-related urban aerosols using Fourier
847 transform ion cyclotron resonance mass spectrometry, *Atmos. Chem. Phys.*, 20, 6803-
848 6820, <https://doi.org/10.5194/acp-20-6803-2020>, 2020.

849 Xu, Y. and Xiao, H.: Concentrations and nitrogen isotope compositions of free
850 amino acids in *Pinus massoniana* (Lamb.) needles of different ages as indicators of
851 atmospheric nitrogen pollution, *Atmos. Environ.*, 164, 348-359,
852 <https://doi.org/10.1016/j.atmosenv.2017.06.024>, 2017.

853 Xu, Y., Lin, Z., and Wu, C.: Spatiotemporal Variation of the Burned Area and Its
854 Relationship with Climatic Factors in Central Kazakhstan, *Remote Sens.*, 13, 313,
855 <https://doi.org/10.3390/rs13020313>, 2021.

856 Xu, Y., Dong, X.-N., Xiao, H.-Y., He, C., and Wu, D.-S.: Water-Insoluble
857 Components in Rainwater in Suburban Guiyang, Southwestern China: A Potential
858 Contributor to Dissolved Organic Carbon, *J. Geophys. Res.-Atmos.*, 127,
859 e2022JD037721, <https://doi.org/10.1029/2022JD037721>, 2022a.

860 Xu, Y., Dong, X.-N., Xiao, H.-Y., Zhou, J.-X., and Wu, D.-S.: Proteinaceous
861 Matter and Liquid Water in Fine Aerosols in Nanchang, Eastern China: Seasonal
862 Variations, Sources, and Potential Connections, *J. Geophys. Res.-Atmos.*, 127,
863 e2022JD036589, <https://doi.org/10.1029/2022JD036589>, 2022b.

864 Xu, Y., Dong, X. N., He, C., Wu, D. S., Xiao, H. W., and Xiao, H. Y.: Mist cannon
865 trucks can exacerbate the formation of water-soluble organic aerosol and PM_{2.5}
866 pollution in the road environment, *Atmos. Chem. Phys.*, 23, 6775-6788,
867 <https://doi.org/10.5194/acp-23-6775-2023>, 2023.

868 Xu, Y., Miyazaki, Y., Tachibana, E., Sato, K., Ramasamy, S., Mochizuki, T.,
869 Sadanaga, Y., Nakashima, Y., Sakamoto, Y., Matsuda, K., and Kajii, Y.: Aerosol Liquid
870 Water Promotes the Formation of Water-Soluble Organic Nitrogen in Submicrometer
871 Aerosols in a Suburban Forest, *Environ. Sci. Technol.*, 54, 1406-1414,
872 <https://dx.doi.org/10.1021/acs.est.9b05849>, 2020.

873 Yang, T., Xu, Y., Ye, Q., Ma, Y. J., Wang, Y. C., Yu, J. Z., Duan, Y. S., Li, C. X.,
874 Xiao, H. W., Li, Z. Y., Zhao, Y., and Xiao, H. Y.: Spatial and diurnal variations of aerosol
875 organosulfates in summertime Shanghai, China: potential influence of photochemical
876 processes and anthropogenic sulfate pollution, *Atmos. Chem. Phys.*, 23, 13433-13450,
877 <https://doi.org/10.5194/acp-23-13433-2023>, 2023.

878 Zahardis, J., Geddes, S., and Petrucci, G. A.: The ozonolysis of primary aliphatic
879 amines in fine particles, *Atmos. Chem. Phys.*, 8, 1181-1194,
880 <https://doi.org/10.5194/acp-8-1181-2008>, 2008.

881 Zarzana, K. J., De Haan, D. O., Freedman, M. A., Hasenkopf, C. A., and Tolbert,

882 M. A.: Optical Properties of the Products of α -Dicarbonyl and Amine Reactions in
883 Simulated Cloud Droplets, *Environ. Sci. Technol.*, 46, 4845-4851,
884 <https://doi.org/10.1021/es2040152>, 2012.

885 Zeng, Y., Ning, Y., Shen, Z., Zhang, L., Zhang, T., Lei, Y., Zhang, Q., Li, G., Xu,
886 H., Ho, S. S. H., and Cao, J.: The Roles of N, S, and O in Molecular Absorption Features
887 of Brown Carbon in PM_{2.5} in a Typical Semi-Arid Megacity in Northwestern China, *J.*
888 *Geophys. Res.-Atmos.*, 126, e2021JD034791, <https://doi.org/10.1029/2021JD034791>,
889 2021.

890 Zeng, Y., Shen, Z., Takahama, S., Zhang, L., Zhang, T., Lei, Y., Zhang, Q., Xu, H.,
891 Ning, Y., Huang, Y., Cao, J., and Rudolf, H.: Molecular Absorption and Evolution
892 Mechanisms of PM_{2.5} Brown Carbon Revealed by Electrospray Ionization Fourier
893 Transform-Ion Cyclotron Resonance Mass Spectrometry During a Severe Winter
894 Pollution Episode in Xi'an, China, *Geophys. Res. Lett.*, 47, e2020GL087977,
895 <https://doi.org/10.1029/2020GL087977>, 2020.

896 Zhang, B., Shen, Z., He, K., Sun, J., Huang, S., Xu, H., Li, J., Ho, S. S. H., and
897 Cao, J.-j.: Insight into the Primary and Secondary Particle-Bound Methoxyphenols and
898 Nitroaromatic Compound Emissions from Solid Fuel Combustion and the Updated
899 Source Tracers, *Environ. Sci. Technol.*, 57, 14280-14288, 10.1021/acs.est.3c04370,
900 2023.

901 Zhang, Q., Jimenez, J. L., Canagaratna, M. R., Allan, J. D., Coe, H., Ulbrich, I.,
902 Alfarra, M. R., Takami, A., Middlebrook, A. M., Sun, Y. L., Dzepina, K., Dunlea, E.,
903 Docherty, K., DeCarlo, P. F., Salcedo, D., Onasch, T., Jayne, J. T., Miyoshi, T., Shiono,

904 A., Hatakeyama, S., Takegawa, N., Kondo, Y., Schneider, J., Drewnick, F., Borrmann,
905 S., Weimer, S., Demerjian, K., Williams, P., Bower, K., Bahreini, R., Cottrell, L., Griffin,
906 R. J., Rautiainen, J., Sun, J. Y., Zhang, Y. M., and Worsnop, D. R.: Ubiquity and
907 dominance of oxygenated species in organic aerosols in anthropogenically-influenced
908 Northern Hemisphere midlatitudes, *Geophys. Res. Lett.*, 34,
909 <https://doi.org/10.1029/2007GL029979>, 2007.

910 Zhang, T., Shen, Z., Huang, S., Lei, Y., Zeng, Y., Sun, J., Zhang, Q., Ho, S. S. H.,
911 Xu, H., and Cao, J.: Optical properties, molecular characterizations, and oxidative
912 potentials of different polarity levels of water-soluble organic matters in winter PM_{2.5}
913 in six China's megacities, *Sci. Total Environ.*, 853, 158600,
914 <https://doi.org/10.1016/j.scitotenv.2022.158600>, 2022.

915 Zhao, Y., Hu, M., Slanina, S., and Zhang, Y.: Chemical Compositions of Fine
916 Particulate Organic Matter Emitted from Chinese Cooking, *Environ. Sci. Technol.*, 41,
917 99-105, <https://doi.org/10.1021/es0614518>, 2007.

918 Zhong, S., Chen, S., Deng, J., Fan, Y., Zhang, Q., Xie, Q., Qi, Y., Hu, W., Wu, L.,
919 Li, X., Pavuluri, C. M., Zhu, J., Wang, X., Liu, D., Pan, X., Sun, Y., Wang, Z., Xu, Y.,
920 Tong, H., Su, H., Cheng, Y., Kawamura, K., and Fu, P.: Impact of biogenic secondary
921 organic aerosol (SOA) loading on the molecular composition of wintertime PM_{2.5} in
922 urban Tianjin: an insight from Fourier transform ion cyclotron resonance mass
923 spectrometry, *Atmos. Chem. Phys.*, 23, 2061-2077, [https://doi.org/10.5194/acp-23-](https://doi.org/10.5194/acp-23-2061-2023)
924 [2061-2023](https://doi.org/10.5194/acp-23-2061-2023), 2023.

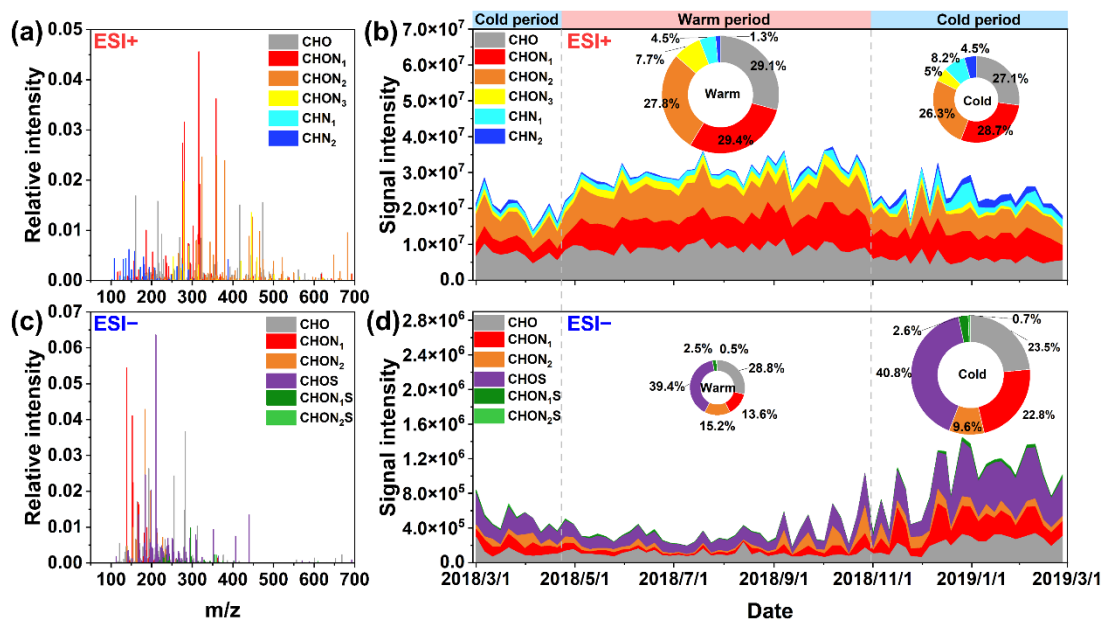
925 Zhou, S., Guo, F., Chao, C.-Y., Yoon, S., Alvarez, S. L., Shrestha, S., Flynn, J. H.,

926 III, Usenko, S., Sheesley, R. J., and Griffin, R. J.: Marine Submicron Aerosols from the
927 Gulf of Mexico: Polluted and Acidic with Rapid Production of Sulfate and
928 Organosulfates, *Environ. Sci. Technol.*, 57, 5149-5159,
929 <https://doi.org/10.1021/acs.est.2c05469>, 2023.

930 Zou, C., Cao, T., Li, M., Song, J., Jiang, B., Jia, W., Li, J., Ding, X., Yu, Z., Zhang,
931 G., and Peng, P.: Measurement report: Changes in light absorption and molecular
932 composition of water-soluble humic-like substances during a winter haze bloom-decay
933 process in Guangzhou, China, *Atmos. Chem. Phys.*, 23, 963-979,
934 <https://doi.org/10.5194/acp-23-963-2023>, 2023.

935

936 **Figure 1.**



937

938 **Figure 1.** The reconstructed mass spectrum distribution of the detected species in PM_{2.5}

939 in (a) ESI+ and (c) ESI- modes during the whole campaign. Temporal variations in the

940 fractional distribution of classified compounds in (b) ESI+ and (d) ESI- modes. The

941 ring diagrams inside the panel show the signal intensity fractions of classified

942 compounds, the size of which is proportional to the total signal intensity of all species

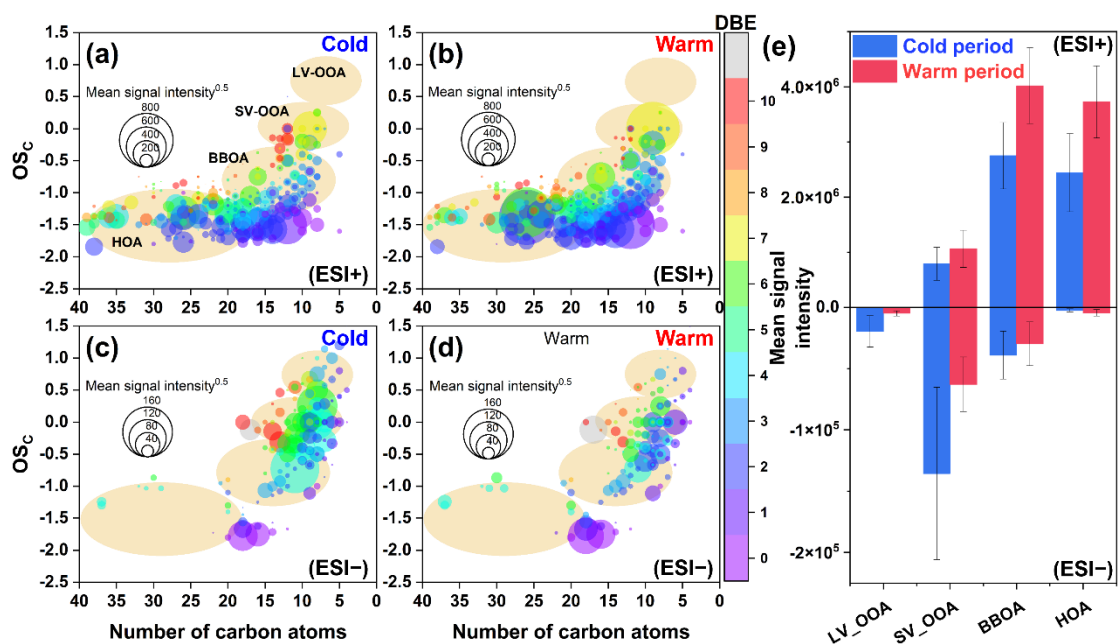
943 detected in PM_{2.5} in different periods.

944

945

946

947 **Figure 2.**



948

949 **Figure 2.** OSc values of CHO molecules detected in (a and b) ESI+ and (c and d) ESI-

950 modes in PM_{2.5} collected from different periods (cold vs. warm). The size and color of

951 the circle indicate the mean signal intensity and DBE value of compounds, respectively.

952 The light-orange background indicates the areas of low-volatility oxidized OA (LV-

953 OOA), semivolatile oxidized OA (SV-OOA), biomass burning-like OA (BBOA), and

954 hydrocarbon-like OA (HOA) (Kroll et al., 2011), according to which (e) the mean signal

955 intensity of classified compounds was calculated for samples from different periods.

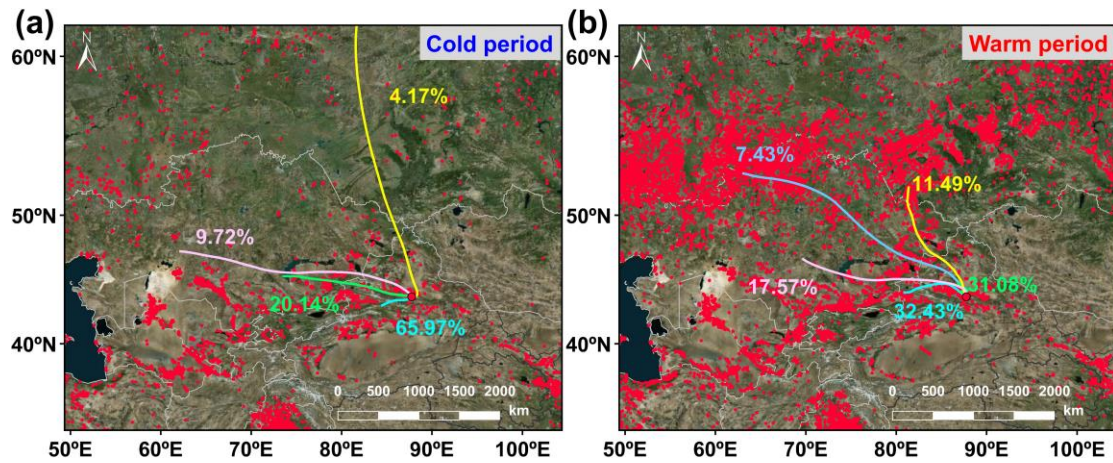
956

957

958

959

960 **Figure 3**



961

962 **Figure 3.** The 3-day (72 h) back trajectories illustrating the typical air mass flows to

963 the study site during the (a) warm and (b) cool periods. Fire spots were shown in red,

964 which was created based on NASA active fire data (VIIRS 375 m,

965 https://firms.modaps.eosdis.nasa.gov/active_fire/). The map was derived from

966 ©MeteoInfoMap (version 3.6.2) (Chinese Academy of Meteorological Sciences, China).

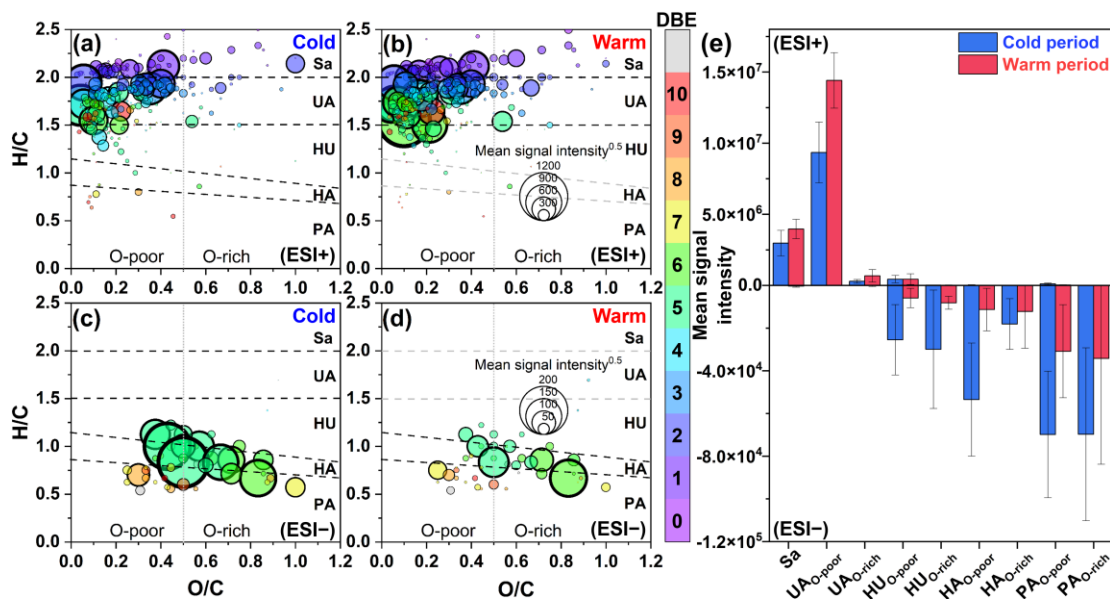
967

968

969

970

971 **Figure 4.**



972

973 **Figure 4.** Van Krevelen diagrams of CHON molecules detected in (a and b) ESI+ and
974 (c and d) ESI- modes in PM_{2.5} collected from different periods (cold vs. warm). The
975 subgroups in the panel include saturated-like (Sa), unsaturated aliphatic-like (UA),
976 highly unsaturated-like (HU), highly aromatic-like (HA), and polycyclic aromatic-like
977 (PA) compounds, further distinguishing between oxygen-poor and oxygen-rich
978 compounds with an oxygen to carbon ratio of 0.5. The size and color of the circle
979 indicate the mean signal intensity and DBE value of compounds, respectively. The (e)
980 mean signal intensity of classified compounds was calculated for samples from
981 different periods.

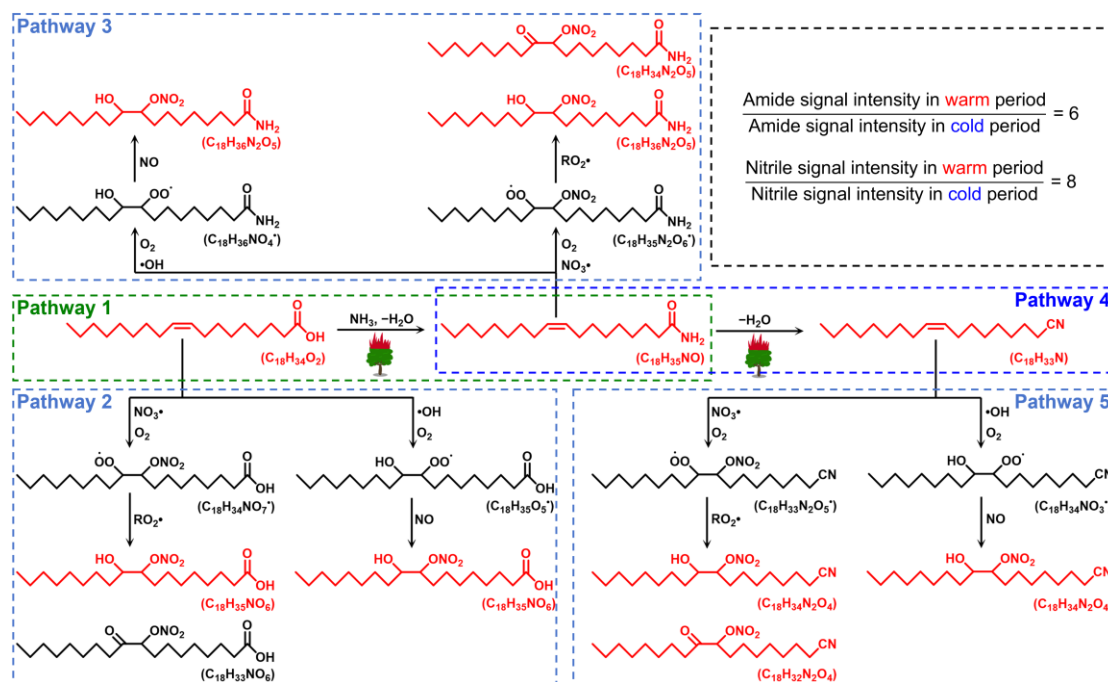
982

983

984

985

986 **Figure 5.**

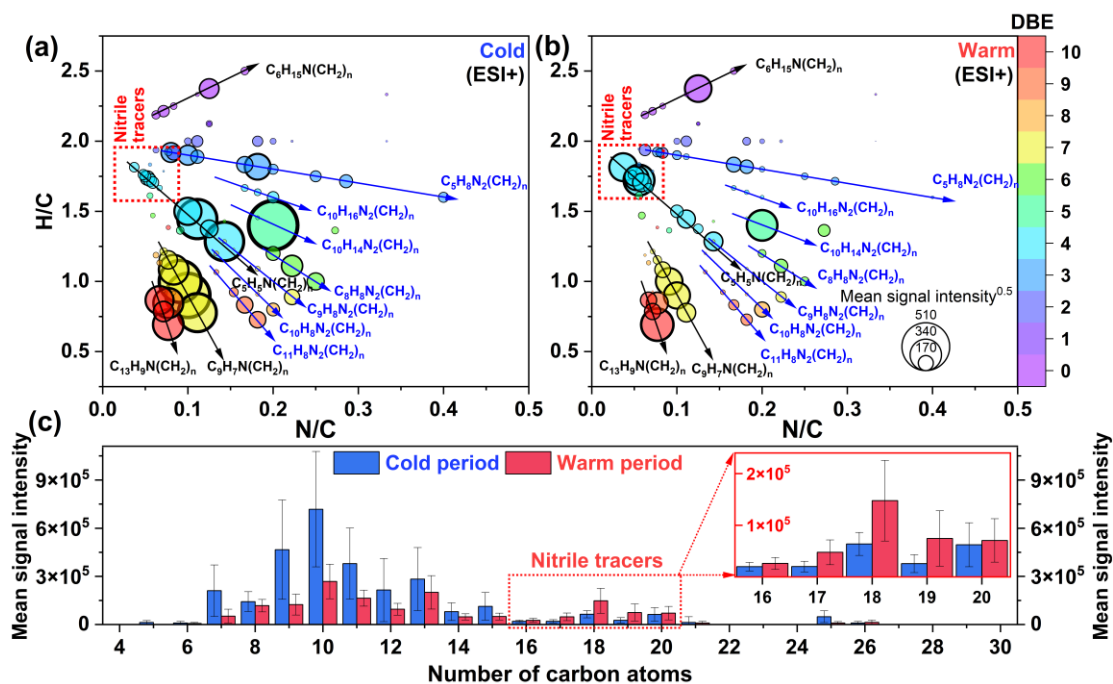


987

988 **Figure 5.** Proposed pathways for the reactions of carboxylic acids (oleic acid as a
 989 representative) with reactive nitrogen and atmospheric oxides to form the observed
 990 NOCs in PM_{2.5} under the influence of the high temperature generated during wildfires
 991 or forest fires. Compounds observed in PM_{2.5} were shown in red.

992

993 **Figure 6.**

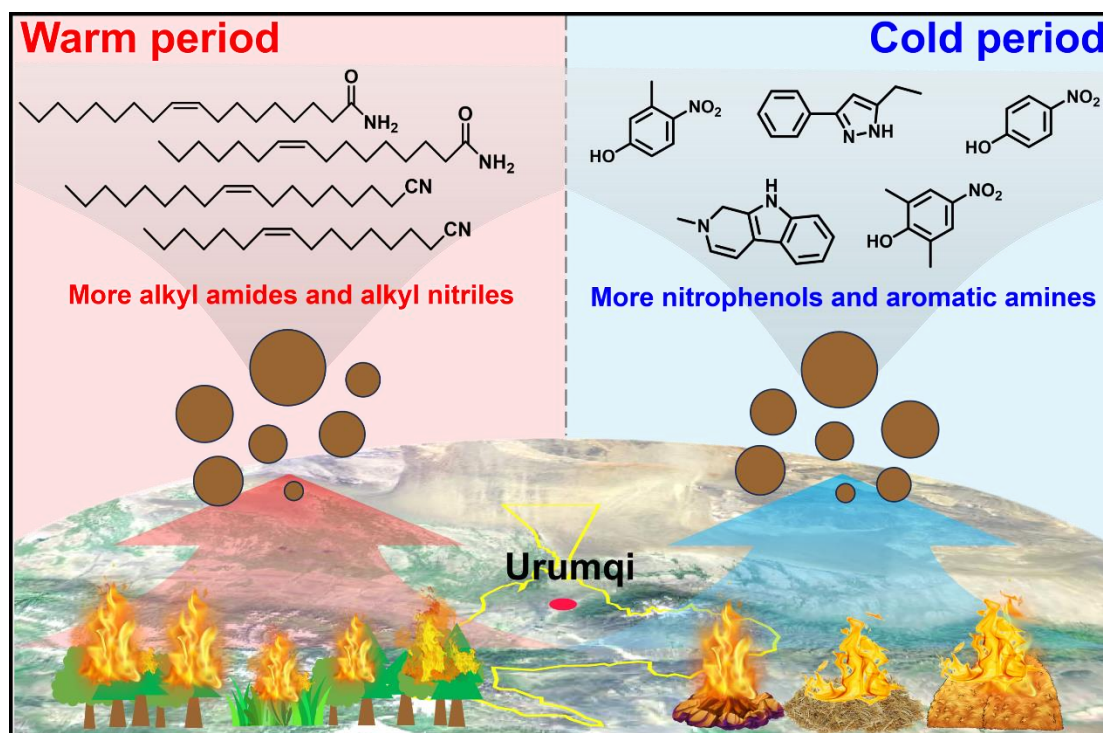


994

995 **Figure 6.** Van Krevelen diagrams of CHN molecules detected in PM_{2.5} collected from
 996 the (a) cold and (b) warm periods. The size and color of the circle indicate the mean
 997 signal intensity and DBE value of compounds, respectively. The mean signal intensity
 998 distributions of (c) carbon atoms in CHN molecules detected in PM_{2.5} collected from
 999 the cold and warm periods

1000

1001 **Figure 7.**



1002

1003 **Figure 7.** Conceptual picture showing the differential impacts of combustion of fresh
1004 and old-age biomass materials on aerosol NOCs in suburban Urumqi. The map was
1005 derived from ©Baidu Maps (BIDU, China).